

# Design Optimization of Transformerless Grid-Connected PV Inverters Including Reliability

Eftichios Koutroulis, *Member, IEEE*, and Frede Blaabjerg, *Fellow, IEEE*

**Abstract**—This paper presents a new methodology for optimal design of transformerless photovoltaic (PV) inverters targeting a cost-effective deployment of grid-connected PV systems. The optimal switching frequency as well as the optimal values and types of the PV inverter components is calculated such that the PV inverter LCOE generated during the PV system lifetime period is minimized. The LCOE is also calculated considering the failure rates of the components, which affect the reliability performance and lifetime maintenance cost of the PV inverter. A design example is presented, demonstrating that compared to the nonoptimized PV inverter structures, the PV inverters designed using the proposed optimization methodology exhibit lower total manufacturing and lifetime maintenance cost and inject more energy into the electric-grid and by that minimizing LCOE.

**Index Terms**—DC-AC power conversion, failure analysis, optimization methods, photovoltaic (PV) power systems, reliability.

## NOMENCLATURE

$C_f$	$LCL$ -filter capacitor.	$P_{1ps,i}$	Total power loss of the $i$ th power switch.
$C_{inv}(\mathbf{X})$	Present value of the PV inverter total cost.	$P_{l,R_{dr}}$	Power loss of the $LCL$ -filter damping resistor.
$C_t(\mathbf{X})$	Total manufacturing cost of the PV inverter.	$P_M(t)$	PV array power production at the maximum power point during hour $t$ .
$E_i(\mathbf{X})$	Total energy injected into the electric grid.	$P_n$	Nominal output power of the PV inverter.
$L$	Converter-side inductance.	$P_o$	Power injected into the electric grid.
LCOE	Levelized cost of the electricity generated.	$\frac{P_{pv}}{P_{R_{dr}}}$	Output power of the PV array.
$L_g$	Grid-side inductance.	$P_{tot}$	Weighted-average value of the damping resistor power consumption.
$M_{inv}$	Repair cost of the PV inverter.	$R_{dr}$	Total power loss of the PV inverter.
$M_t(\mathbf{X})$	Present value of the total maintenance cost.	$RF_{max}$	$LCL$ -filter damping resistor.
$N_j(\mathbf{X})$	Average number of failures during the $j$ th year of operation.	$R_p(\mathbf{X})$	Maximum permissible limit of harmonic current distortion at the PV inverter output.
$P_{d,max}$	Maximum power dissipated in the damping resistor.	$SF$	Reliability (or survival) function.
$P_{cu}$	Power consumption of the PV inverter control unit.	$S_l$	Damping resistor oversizing factor.
$P_{ld,i}$	Total power loss of the $i$ th free-wheeling diode.	$T_A(t, y)$	Radiating surface area of case per unit inductance and per unit nominal operating current.
$P_{l,L}(t, y)$	Power loss of the $LCL$ -filter converter-side inductor.	$\overline{T_A}$	PV inverter ambient temperature at hour $t$ of year $y$ .
$P_{l,L_g}$	Power loss of the $LCL$ -filter grid-side inductor.	$\overline{T_{jd,i}}$	Weighted-average value of the ambient temperature.
		$\overline{T_{jd,max}}$	Weighted-average value of the free-wheeling diodes junction temperature.
		$T_{jnd,i}$	Maximum permissible junction temperature of the free-wheeling diodes.
		$T_{jps,i}$	Operating junction temperature of the free-wheeling diodes.
		$\overline{T_{jps,i}}$	Operating junction temperature of the power switches.
		$T_{jps,max}$	Weighted-average value of the power switches' junction temperature.
		$\overline{T_L}$	Maximum permissible junction temperature of the power switches.
		$\overline{T_{Lg}}$	Weighted-average of the converter-side inductor operating temperature.
		$\overline{T_{R_{dr}}}$	Weighted-average of the grid-side inductor operating temperature.
		$\overline{V_{Cf}}$	Weighted-average of the damping resistor operating temperature.
		$\overline{V_{pv}}$	Weighted-average of the $LCL$ -filter capacitor voltage.
		$V_n$	Weighted-average of the dc input voltage.
		$\mathbf{X}$	Nominal voltage of the electric grid.
		$c_c$	Vector of the optimization problem design variables.
		$c_d$	$LCL$ -filter capacitor cost per unit capacitance.
		$c_{hs}$	Free-wheeling diode cost.
			Cost of the heat sink.

Manuscript received February 3, 2012; revised March 30, 2012; accepted April 30, 2012. Date of current version September 11, 2012. This paper was presented at the 27th Annual IEEE Applied Power Electronics Conference and Exposition, Orlando, FL, February 5–9, 2012. Recommended for publication by Associate Editor P. T. Krein.

E. Koutroulis is with the Department of Electronic and Computer Engineering, Technical University of Crete, Chania GR-73100, Greece (e-mail: efkout@electronics.tuc.gr).

F. Blaabjerg is with the Department of Energy Technology, Aalborg University, Aalborg DK-9220, Denmark (e-mail: fbl@et.aau.dk).

Color versions of one or more of the figures in this paper are available online at <http://ieeexplore.ieee.org>.

Digital Object Identifier 10.1109/TPEL.2012.2198670

$c_i$	$LCL$ -filter inductor cost per unit inductance and current rating.
$c_{inv}$	Partial manufacturing cost of the PV inverter.
$c_r$	Filter damping resistor cost per unit resistance and power.
$c_s$	Power switch cost.
$d$	Annual discount rate.
$f$	Nominal frequency of the electric grid.
$f_s$	Switching frequency.
$f_{s,max}$	Maximum switching speed capability of the power switches.
$g$	Annual inflation rate.
$n$	Number of years of PV system service lifetime.
$p$	Total number of power switches.
$r(\cdot)$	Annual reduction coefficient of the PV modules output power.
$t$	Time number ( $1 \leq t \leq 8760$ ).
$y$	Year number ( $1 \leq y \leq n$ ).
$\Delta t$	Simulation time step.
$\theta_{ca}$	Thermal resistance of the heat sink.
$\theta_{jc,d}$	Thermal resistance from the junction to the case of the free-wheeling diodes.
$\theta_{jc,ps}$	Thermal resistance from the junction to the case of the power switches.
$\lambda_c$	Total failure rate of the remaining components and subsystems of the PV inverter.
$\lambda_{C_f}$	Failure rate of the $LCL$ -filter capacitor.
$\lambda_{C_{in}}$	Failure rate of the dc-link capacitor.
$\lambda_{d,i}$	Failure rate of the free-wheeling diodes.
$\lambda_{inv}(\mathbf{X})$	PV inverter failure rate.
$\lambda_L$	Failure rate of the $LCL$ -filter converter-side inductor.
$\lambda_{L_g}$	Failure rate of the $LCL$ -filter grid-side inductor.
$\lambda_{ps,i}$	Failure rate of the power switches.
$\lambda_{R_{dr}}$	Failure rate of the $LCL$ -filter damping resistor.

## I. INTRODUCTION

ACCORDING to the European Photovoltaic Industry Association, the growth of the photovoltaic (PV) system capacity seen in the last ten years is expected to continue in the near future also [1]. Nowadays, the majority of PV systems are used to supply the generated energy into the electric grid. A block diagram of a grid-connected PV system employing a transformerless, full-bridge dc/ac inverter (PV inverter) is illustrated in Fig. 1. Compared to the PV inverters with galvanic isolation, the transformerless PV inverters have the advantages of lower cost, higher efficiency, smaller size, and lower weight [2], [3]. Using an  $LCL$ -type output filter, instead of the traditional  $L$ - or  $LC$ -type filters, aims toward the reduction of the size of the reactive elements comprising the output filter of the PV inverter [4], [5].

A cost-effective deployment of grid-connected PV systems can be achieved by minimizing the initial investment cost required to purchase and install the PV system components (e.g., PV modules, dc/ac inverters, etc.), maximizing the amount of energy injected into the electric grid, and increasing its reliability

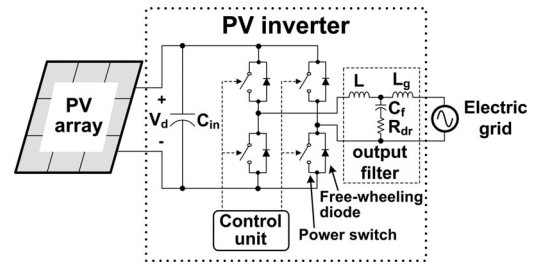


Fig. 1. Grid-connected PV system employing a transformerless PV inverter.

by minimizing the number of failures of the PV system components which occur during the operational lifetime period of the PV installation [6], [7]. The energy injected into the electric grid can be maximized by applying an effective maximum power point tracker (MPPT) control strategy [8] and designing the PV inverter such that the PV array output power is efficiently processed by the PV inverter [9]. The reliability characteristics of the PV system components are usually expressed using indices such as the failure rate or the mean time between failures (MTBF) [7]. The duration of grid-connected PV system investments follows the operational lifetime period of the commercially available PV modules and it is typically of the order of 25 years. The components comprising the PV system (i.e., PV modules, dc/ac inverters, and the balance of system components) are required to operate with high reliability during that time interval.

The exploration of the PV system components' reliability characteristics is indispensable in order to accurately predict the lifetime energy production and total revenues achieved by the PV energy production system. The commercially available PV modules are typically offered with a 25-year performance warranty and constitute the most reliable component of a PV system [10]. In contrast, according to the analysis presented in [11] where both wearout mechanisms of the components (due to stress factors such as, e.g., the operating temperature) and failures due to inadequate protection (e.g., from surge voltages of the electric grid) were taken into account, the PV inverters are considered as the most vulnerable subsystem of a PV plant. Their reliability is affected by the operational characteristics of the components they comprise, which also affect the PV inverter power conversion efficiency and the amount of energy injected into the electric grid. A single PV inverter failure may cause a significant PV power production loss [12], affecting both the PV plant operating and maintenance costs and the energy yield [13]. As analyzed in [14], the range of ambient temperature values prevailing at the PV inverter installation site, as well as the operating hours and output power levels, must be considered during the PV inverter design stage in order to meet the long-term reliability requirements of the PV inverter. Achieving a high reliability of PV inverters is considered as an immediate priority for the PV industry in order to match the lifetime of PV modules [15]. According to [16], both cost and reliability should be taken into account in order to design PV power processing systems, but frequently the impact of reliability is not explicitly

incorporated in the design process of PV inverters (e.g., such as in [17] and [18]).

The failure mechanisms and reliability modeling approaches of power devices used in power converters are analyzed in [19]. The development of a simulation tool for determining the component temperature and expected reliability of three-phase dc/ac inverters deployed in hybrid electric vehicles is presented in [20]. The reliability of parallel-connected dc/ac inverters operating under a dynamic power distribution control scheme in an  $N+X$  architecture (i.e., the system operates when  $N$  of the total  $N+X$  converters operate) is explored in [21]. The reliability analysis is then used to determine the optimal values of  $N$  and  $X$  such that the total cost of the system is minimized. A procedure for reliability assessment, in terms of the mean time to failure (MTTF) metric, of multiphase dc/dc converters used in PV applications is proposed in [22].

A methodology based on the design-of-experiment (DOE) technique for the design of a PV inverter such that it exhibits the desired MTBF is presented in [23]. The reliability of various topologies for a module-integrated PV inverter is investigated in [24] based on the MTBF metric. In [25], a technique is presented for the calculation of the MTBF of the dc input capacitors employed in a module-integrated PV inverter. The operating temperature of the capacitors is predicted by utilizing a heat-flow thermal model of the PV modules. The cost and failure rates of the dc-link capacitor and power MOSFETs used in various single-phase PV inverter topologies, which are capable of providing reactive power support, are further explored in [26]. The reliability estimation of two-stage, three-stage, and boost inverter topologies used in grid-connected PV systems, together with a sensitivity analysis of reliability in terms of the power switches type, dc input capacitor voltage rating, and ambient temperature, is presented in [27].

In [28] the number of failures that the PV inverter is expected to encounter during its service lifetime period is predicted using a Monte Carlo analysis. The failure rates of the subsystems corresponding to the PV inverter major failure modes are considered, such as the cooling fans of the power-conditioning unit, the insulated gate bipolar transistors (IGBTs) comprising the power stage, and the energy-storage capacitors. It is demonstrated that the PV inverter availability can be improved by either increasing the repair rate in the case of malfunction or reducing the failure rate of the dc-bus capacitors, which constitute the most vulnerable components of the PV inverter, by designing the PV inverter using capacitors of higher quality. A Monte Carlo simulation-based approach is also presented in [12] for the calculation of the PV inverter availability. It is based on an analysis of the thermal stress imposed on the PV inverter components due to the ambient temperature conditions prevailing at the PV system installation site.

A Bayesian estimation technique is analyzed in [29] for predicting the availability of a PV inverter, which is based on treating the failure and repair rates of the PV inverter as random variables. The use of Markov reliability models is proposed in [30] for exploring the effect of the PV inverter reliability characteristics into the resulting energy yield. The analysis is performed at the PV inverter system level without investigating

the effects of the PV inverter component values and operational characteristics on the PV inverter reliability features.

The methods described previously have been focused on the exploration and improvement of the reliability performance of the PV inverters. However, the impact of reliability on the PV inverter lifetime-cost/energy-production tradeoff has not been investigated. Hence, these approaches do not constitute a systematic procedure enabling the optimal selection of the PV inverter component types and values which will guarantee the development of the most cost-effective PV inverter configuration seen during a lifetime.

In this paper, a new methodology for the optimal design of transformerless PV inverters is presented taken into account reliability. The optimal switching frequency as well as the optimal values and types of the components comprising the PV inverter is calculated such that the PV inverter Levelized Cost Of the Electricity (LCOE) generated is minimized. The number of failures of the components, affecting the PV inverter maintenance cost during the PV system operational lifetime period, is also considered in the LCOE calculation, thus incorporating the impact of their performance in terms of reliability. In contrast to the past-proposed design methods, the approach presented in this paper facilitates the optimal design of the PV inverter based on a systematic process.

In the following sections of this paper, the proposed optimal design methodology and PV inverter modeling for optimization including reliability are analyzed. The features of the proposed methodology are then demonstrated through a design optimization example.

## II. PROPOSED DESIGN OPTIMIZATION METHODOLOGY

With reference to Fig. 1, the target of the proposed design optimization procedure is to calculate the optimal value of the PV inverter switching frequency  $f_s$ , the optimal values of the output filter components (i.e.,  $L$ ,  $L_g$ ,  $C_f$ , and  $R_{dr}$ ), and the optimal types of the power semiconductors including heat sink. The vector of the optimization problem design variables  $\mathbf{X}$  is of the form  $\mathbf{X} = [L|L_g|C_f|f_s]$ . The optimal value of the LCL-filter damping resistor  $R_{dr}$  is calculated using the resulting optimal values of  $L$ ,  $L_g$ , and  $C_f$ , as analyzed in [5].

A block diagram of the proposed automated optimization procedure is illustrated in Fig. 2. The optimization algorithm inputs provided by the PV inverter designer are: 1) the input-output specifications, topology, and modulation strategy of the PV inverter; 2) the technical and economical characteristics of multiple alternative types of components (i.e., power semiconductors, heat sinks, inductors, etc.) used to build the PV inverter; 3) the grid-interconnection specifications (e.g., maximum permitted harmonic current levels, etc.); 4) the operational characteristics of the PV array connected to the PV inverter; and 5) the 1-h average solar irradiance and ambient temperature time-series during the year.

During the optimization process, new sets of values of the design variables are iteratively produced by the optimization algorithm. Then, the objective function is evaluated using the appropriate mathematical model of the PV inverter topology

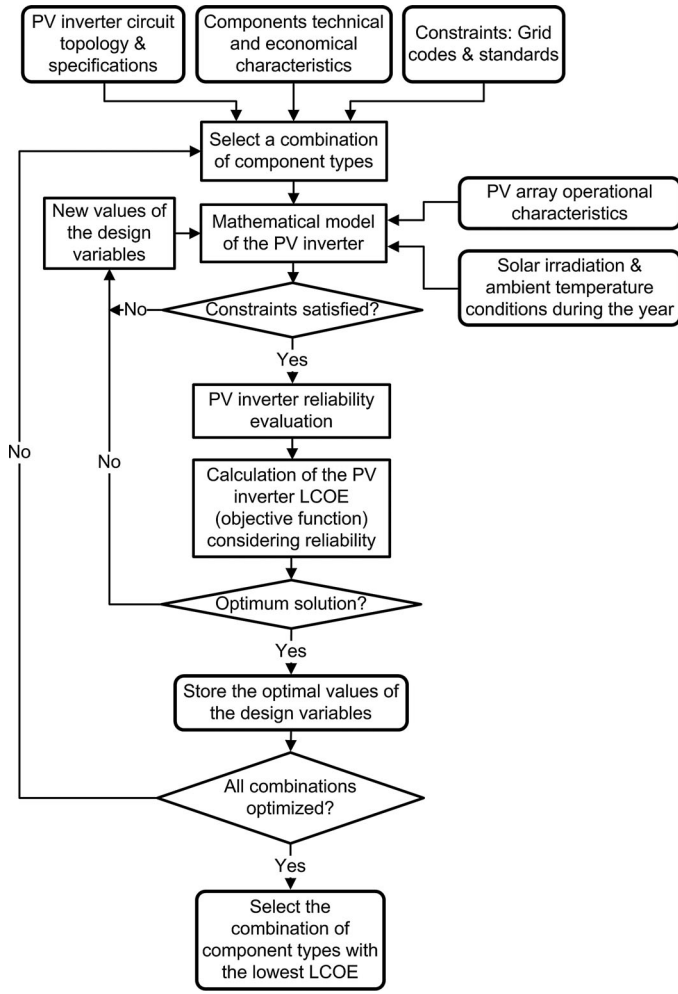


Fig. 2. Flowchart of the proposed optimization procedure.

under consideration, only for those sets of design variables satisfying the PV inverter operational constraints. The reliability features of the PV inverter components are also considered during this stage, as analyzed next. This process is repeated until the global optimum of the objective function has been derived. The optimization procedure is implemented using genetic algorithms, which are capable to derive the global optimum solution of the objective function with computational efficiency. The PV inverter optimal design process described previously is repeated for all combinations of component types input by the PV inverter designer (e.g., multiple alternative types of power switches such as IGBTs and MOSFETs, or IGBT-type power switches mounted on alternative heat sink structures available in the market, each with a different thermal resistance to ambient, etc.). The combination achieving the lowest optimal value of the objective function and the corresponding values of the design variables is output as the overall optimal configuration of the PV inverter.

The optimal values of the design variables are calculated such that the PV inverter LCOE generated [31], LCOE (€/Wh), is

minimized by

$$\text{minimize } \{ \text{LCOE}(\mathbf{X}) \}$$

subject to: design specifications and constraints are met (1)

where

$$\text{LCOE}(\mathbf{X}) = \frac{C_{\text{inv}}(\mathbf{X})}{E_i(\mathbf{X})} \quad (2)$$

with  $C_{\text{inv}}(\mathbf{X})$  (€) being the present value of the PV inverter total cost during its operational lifetime period,  $E_i(\mathbf{X})$  (Wh) being the total energy injected into the electric grid by the PV inverter during its operational lifetime period, and  $\mathbf{X}$  being the vector of the design variables.

The present value of the PV inverter total cost  $C_{\text{inv}}(\mathbf{X})$  is calculated as the sum of the PV inverter manufacturing cost  $C_t(\mathbf{X})$  (€) and the present value of the total maintenance cost during the PV inverter operational lifetime period  $M_t(\mathbf{X})$  (€)

$$C_{\text{inv}}(\mathbf{X}) = C_t(\mathbf{X}) + M_t(\mathbf{X}). \quad (3)$$

The total maintenance cost  $M_t$  depends on the PV inverter reliability characteristics. The values of  $C_t$ ,  $M_t$ , and  $E_i$  in (2) and (3) are calculated according to the PV inverter modeling analyzed in the following.

### III. PV INVERTER MODELING FOR OPTIMIZATION INCLUDING RELIABILITY

The PV inverter total manufacturing cost  $C_t$  is equal to the sum of the prices of the individual components comprising the PV inverter

$$C_t(\mathbf{X}) = c_{\text{inv}} P_n + c_{\text{hs}} + p \cdot (c_s + c_d) + c_i \cdot (L + L_g) \frac{P_n}{V_n} + c_c C_f + SF \cdot c_r R_{\text{dr}} P_{d,\text{max}} \quad (4)$$

where  $c_{\text{inv}}$  (€/W) is the PV inverter manufacturing cost without including the cost of the heat sink, power switches, diodes, and output filter components (e.g., control unit, printed circuit boards, enclosure, etc.),  $c_{\text{hs}}$  (€) is the cost of the heat sink,  $p$  is the number of power switches and free-wheeling diodes contained in the PV inverter power section,  $c_s$  and  $c_d$  (€) are the cost of each power switch and free-wheeling diode, respectively,  $c_i$  [€/ (H · A)] is the LCL-filter inductor cost per unit inductance and current rating,  $c_c$  (€/F) is the filter capacitor cost per unit capacitance,  $c_r$  [€/ (Ω · W)] is the filter damping resistor cost per unit resistance and power,  $SF$  (%) is the damping resistor oversizing factor, and  $P_{d,\text{max}}$  (W) is the maximum power dissipated in the damping resistor during the PV system operational lifetime period.

The present value of the PV inverter total maintenance cost  $M_t$  depends on the PV inverter reliability performance during its operational lifetime period and it is determined by the type and values of the individual components comprising the PV inverter. The value of  $M_t$  is calculated by reducing the future expenses for repairing the PV inverter to the corresponding present value,

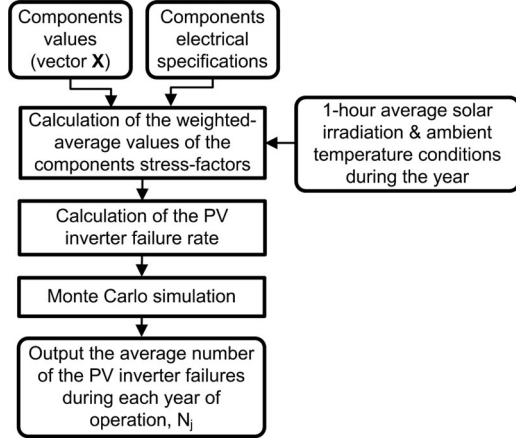


Fig. 3. PV inverter reliability evaluation procedure.

according to the following equation:

$$M_t(\mathbf{X}) = \sum_{j=1}^n N_j(\mathbf{X}) \cdot M_{\text{inv}} \cdot \frac{(1+g)^j}{(1+d)^j} \quad (5)$$

where  $n$  is the number of years of PV system service lifetime,  $N_j(\mathbf{X})$  is the average number of failures that the PV inverter is expected to encounter during the  $j$ th year of operation ( $1 \leq j \leq n$ ),  $M_{\text{inv}}(\text{€})$  is the present value of the cost for repairing the PV inverter,  $g$  (%) is the annual inflation rate, and  $d$  (%) is the annual discount rate.

The values of  $N_j(\mathbf{X})$  are calculated for each set of the component values (i.e., vector  $\mathbf{X}$ ) produced during the GA-based optimization process, according to the PV inverter reliability evaluation flowchart illustrated in Fig. 3. The failure rate of a component depends on the value of the component and the stress factor applied to it (e.g., PV inverter dc input voltage, ambient temperature, etc.) [32]. However, the PV inverter operates under stochastically varying solar irradiation and ambient temperature conditions during the year, resulting in time-variable values of the stress factors. Thus, in the proposed methodology the average values of the stress factors developed at each component during the year, weighted by the percentage of operating hours at each stress level, are initially calculated. This task is accomplished using the mathematical model of the PV inverter, which is analyzed next, and the 1-h average solar irradiance and ambient temperature time-series during the year input by the PV inverter designer. Then, the failure rate of the PV inverter is calculated by applying the weighted-average values of the stress factors in the individual component failure-rate models described in [28] and [32]. Using the resulting value of the PV inverter failure rate, the average number of failures during each year of operation  $N_j(\mathbf{X})$  is calculated by performing a Monte Carlo simulation with 10 000 samples.

The probability that the PV inverter will operate properly beyond time  $t$  is expressed by the reliability (or survival) function  $R_p(\mathbf{X})$  which is given by [21], [33]

$$R_p(\mathbf{X}) = e^{-\lambda_{\text{inv}}(\mathbf{X}) \cdot t} \quad (6)$$

where  $\lambda_{\text{inv}}(\mathbf{X})$  (number of failures/10<sup>6</sup> h) is the PV inverter failure rate.

The value of  $\lambda_{\text{inv}}(\mathbf{X})$  is calculated for each set of values of the design variables  $\mathbf{X}$  as the sum of the failure rates of the individual components comprising the PV inverter, as follows:

$$\begin{aligned} \lambda_{\text{inv}}(\mathbf{X}) = & \sum_{i=1}^p [\lambda_{\text{ps},i}(\overline{T_{\text{jps},i}}) + \lambda_{\text{d},i}(\overline{T_{\text{jnd},i})] + \lambda_L(\overline{T_L}) \\ & + \lambda_{L_g}(\overline{T_{L_g}}) + \lambda_{C_f}(C_f, \overline{V_{C_f}}, \overline{T_A}) + \lambda_{R_{\text{dr}}}(\overline{P_{R_{\text{dr}}}}, \overline{T_{R_{\text{dr}}}}) \\ & + \lambda_{C_{\text{in}}}(C_{\text{in}}, \overline{V_{\text{pv}}}, \overline{T_A}) + \lambda_c \end{aligned} \quad (7)$$

where  $\lambda_{\text{ps},i}$ ,  $\lambda_{\text{d},i}$  ( $1 \leq i \leq p$ ),  $\lambda_L$ ,  $\lambda_{L_g}$ ,  $\lambda_{C_f}$ , and  $\lambda_{R_{\text{dr}}}$  are the failure rates (number of failures/10<sup>6</sup> h) of the PV inverter power switches, free-wheeling diodes,  $LCL$ -type output filter inductors ( $L$  and  $L_g$ ), capacitor ( $C_f$ ), and damping resistor ( $R_{\text{dr}}$ ), respectively,  $\lambda_{C_{\text{in}}}$  is the failure rate of the dc-link capacitor,  $\lambda_c$  is the total failure rate of the remaining components and subsystems of the PV inverter (e.g., FPGA or DSP boards of the control unit, monitoring sensors, etc.),  $\overline{T_A}$  is the weighted-average value of ambient temperature, and  $\overline{V_{\text{pv}}}$ ,  $\overline{V_{C_f}}$ ,  $\overline{P_{R_{\text{dr}}}}$ ,  $\overline{T_{\text{jps},i}}$ ,  $\overline{T_{\text{jnd},i}}$ ,  $\overline{T_L}$ ,  $\overline{T_{L_g}}$ , and  $\overline{T_{R_{\text{dr}}}}$  are the weighted-average values of the PV inverter dc input voltage (i.e., PV array output voltage),  $LCL$ -filter capacitor voltage, damping resistor power consumption and operating temperature levels of the power switches, free-wheeling diodes, and  $LCL$ -filter components (i.e.,  $L$ ,  $L_g$ , and  $R_{\text{dr}}$ ), respectively.

Similarly to [28], [34], the total failure rate of the PV inverter components not included in the set of the PV inverter design variables (e.g., FPGA or DSP boards, monitoring sensors, etc.)  $\lambda_c$  is considered to be constant throughout the PV plant lifetime period. The dc-link capacitor and control unit are not included in the set  $\mathbf{X}$  of the design variables of the proposed optimization process. The value of the dc-link capacitor is calculated such that the voltage ripple at the PV array output is reduced to an acceptable level, using the methodology analyzed in [35]. However, the resulting value of dc-link capacitance, as well as the control unit, affects the reliability performance of the PV inverter. Thus, their failure rates are included in (7) for the calculation of the total PV inverter failure rate since they affect the statistical behavior of the PV inverter availability throughout its operational lifetime period. The junction temperatures of the power semiconductors,  $T_{\text{jps},i}$  and  $T_{\text{jnd},i}$  (°C), respectively, are calculated assuming that the power switches and diodes are mounted on a common heat sink, using the following equations:

$$\begin{aligned} T_{\text{jps},i}(t, y) = & T_A(t, y) + \theta_{\text{jc,ps}} \cdot P_{\text{ps},i}(t, y) \\ & + \theta_{\text{ca}} \cdot \sum_{j=1}^p [P_{\text{ps},j}(t, y) + P_{\text{ld},j}(t, y)] \end{aligned} \quad (8)$$

$$\begin{aligned} T_{\text{jnd},i}(t, y) = & T_A(t, y) + \theta_{\text{jc,d}} \cdot P_{\text{ld},i}(t, y) \\ & + \theta_{\text{ca}} \cdot \sum_{j=1}^p [P_{\text{ps},j}(t, y) + P_{\text{ld},j}(t, y)] \end{aligned} \quad (9)$$

where  $T_A(t, y)$  (°C) is the PV inverter ambient temperature at hour  $t$  ( $1 \leq t \leq 8760$ ) of year  $y$  ( $1 \leq y \leq n$ ),  $\theta_{\text{jc,ps}}$  and  $\theta_{\text{jc,d}}$  (°C/W) are the thermal resistance from the junction to the case

of the power switches and free-wheeling diodes, respectively,  $\theta_{ca}$  ( $^{\circ}\text{C}/\text{W}$ ) is the thermal resistance of the heat sink, and  $P_{\text{ps},i}$  and  $P_{\text{ld},i}$  (W) are the total power loss (including conduction and switching power losses) of the  $i$ th ( $1 \leq i \leq p$ ) power switch and free-wheeling diode, respectively.

Additionally, in order to ensure that the junction temperature of the power semiconductors employed in the optimized PV inverter structure is less than the maximum operating limit specified by their manufacturer, the proposed optimization process is performed subject to the following constraints:

$$T_{\text{jps},i}(t, y) \leq T_{\text{jps},\text{max}} \quad (10)$$

$$T_{\text{jld},i}(t, y) \leq T_{\text{jld},\text{max}} \quad (11)$$

where  $T_{\text{jps},\text{max}}$  and  $T_{\text{jld},\text{max}}$  ( $^{\circ}\text{C}$ ) are the maximum permissible junction temperatures of the power switches and diodes, respectively.

The reliability calculation procedure is performed using the complete time-series of the hourly average values of solar irradiation and ambient temperature during the year (i.e., 8760 values for each parameter), input by the PV inverter designer. During the time periods that the PV inverter operation is suspended (e.g., during the night hours), the junction temperature of the power semiconductors is calculated from (8) and (9) to follow the ambient temperature.

The operating temperature of the *LCL*-type output filter inductors,  $T_L$  and  $T_{L_g}$ , respectively, is calculated as [32]

$$T_L(t, y) = T_A(t, y) + 1.1 \cdot 125 \cdot P_{l,L}(t, y) \cdot V_n / (S_l \cdot L \cdot P_n) \quad (12)$$

$$T_{L_g}(t, y) = T_A(t, y) + 1.1 \cdot 125 \cdot P_{l,L_g}(t, y) \cdot V_n / (S_l \cdot L_g \cdot P_n) \quad (13)$$

where  $P_{l,L}(t, y)$  and  $P_{l,L_g}(t, y)$  (W) are the power losses (including copper and core losses) of the inductors  $L$  and  $L_g$ , respectively,  $V_n$  (V) and  $P_n$  (W) are the PV inverter nominal output voltage and power levels, respectively, and  $S_l$  [ $\text{m}^2/(\text{H}\cdot\text{A})$ ] is the filter inductors radiating surface area of case per unit inductance and per unit nominal operating current.

In (8)–(13), the parameters  $T_A(t, y)$ ,  $\theta_{\text{jc,ps}}$ ,  $\theta_{\text{jc,d}}$ ,  $\theta_{ca}$ ,  $T_{\text{jps},\text{max}}$ ,  $T_{\text{jld},\text{max}}$ ,  $V_n$ ,  $P_n$ , and  $S_l$  are provided by the PV inverter designer, while the values of  $P_{\text{ps},i}$ ,  $P_{\text{ld},i}$ ,  $P_{l,L}$ , and  $P_{l,L_g}$  are calculated according to the power loss models described in [36] and [37] using the operational characteristics of the components available in the device datasheet, provided by their manufacturer.

The total energy production,  $E_i(\mathbf{X})$  in (2), is calculated as

$$E_i(\mathbf{X}) = \sum_{y=1}^n \sum_{t=1}^{8760} P_o(t, y) \cdot \Delta t \quad (14)$$

where

$$P_o(t, y) = \begin{cases} 0, & \text{during repair} \\ P_{\text{pv}}(t, y) - P_{\text{tot}}(t, y), & \text{else} \end{cases} \quad (15)$$

and  $P_o$ ,  $P_{\text{pv}}$ , and  $P_{\text{tot}}$  (W) are the power injected into the electric grid by the PV inverter, the PV array output power, and the PV

inverter total power loss, respectively, at hour  $t$  ( $1 \leq t \leq 8760$ ) of year  $y$  ( $1 \leq y \leq n$ ) and  $\Delta t = 1 \text{ h}$  is the simulation time step.

As analyzed in [28], the PV inverter repair time depends on the amount of time required to detect the failure, diagnose the type of malfunction, obtain and install spare parts, test the repair, and reinstall the inverter. In order to calculate the PV array output power  $P_{\text{pv}}$  in (15), it is assumed that an MPPT process is performed by the PV inverter control unit, such that the maximum PV power is supplied to the PV inverter [8]. The PV modules' output power deterioration during their service lifetime period is also considered when calculating the PV array output power, since it affects the values of the stress factors applied to the PV inverter components and the resulting failure rates. As stated in [38], the output power degradation of PV modules tends to be linear with time. Thus, in the proposed methodology the PV array output power  $P_{\text{pv}}$  (W) is calculated as follows:

$$P_{\text{pv}}(t, y) = [1 - y \times r(y)] \cdot P_M(t) \quad (16)$$

where  $y$  is the year number ( $1 \leq y \leq n$ ),  $r(\cdot)$  (%/year) is the annual reduction coefficient of the PV modules output power (if  $y = 1$  then  $r(y) = 0$ , while for  $1 < y \leq n$  its value is specified by the PV modules manufacturer), and  $P_M(t)$  is the PV array power production at the maximum power point during hour  $t$  ( $1 \leq t \leq 8760$ ).

The value of  $P_M$  in (16) is calculated using the PV modules model analyzed in [39], based on the solar irradiation and ambient temperature time-series, and the electrical specifications of the PV modules and their configuration (i.e., connection in series and parallel) within the PV array, which are input in the proposed optimization procedure by the PV inverter designer. The total power loss  $P_{\text{tot}}$  (W) is equal to the sum of the power losses of the components comprising the PV inverter

$$P_{\text{tot}}(t, y) = \sum_{i=1}^p [P_{\text{ps},i}(t, y) + P_{\text{ld},i}(t, y)] + P_{l,L}(t, y) + P_{l,L_g}(t, y) + P_{l,R_{\text{dr}}}(t, y) + P_{\text{cu}} \quad (17)$$

where  $P_{l,R_{\text{dr}}}$  (W) is the power loss of the *LCL*-type output filter damping resistor and  $P_{\text{cu}}$  (W) is the power consumption of the PV inverter control unit (including the digital controller boards, gate drivers, sensors, etc.).

The value of  $P_{l,R_{\text{dr}}}$  in (17) is calculated using the power loss model presented in [36], while the value of  $P_{\text{cu}}$  is constant and it is input to the proposed optimization process by the PV inverter designer.

The power switches of the PV inverter under consideration are controlled according to the sinusoidal pulsewidth modulation (SPWM) principle [40]. Thus, the PV inverter switching frequency  $f_s$  (Hz) is constrained to be an integer multiple of the grid frequency  $f$  (Hz) and simultaneously it also holds that

$$f_s \leq f_{s,\text{max}} \quad (18)$$

where  $f_{s,\text{max}}$  (Hz) is the maximum switching speed capability of the power switches, specified by their manufacturer.

The values of the *LCL*-type output filter components (i.e.,  $L$ ,  $L_g$ ,  $C_f$ , and  $R_{dr}$  in Fig. 1) are calculated by the proposed optimization algorithm according to the design principles described in [5] such that

- 1) the current ripple at the PV inverter output is less than the maximum permissible limit of harmonic current distortion at the PV inverter output  $RF_{max}$  (%) which is imposed by the grid regulations and standards;
- 2) the *LCL*-filter resonant frequency is between ten times the electric grid frequency and one-half of  $f_s$ , in order to ensure that resonance problems are avoided;
- 3) the total value of the PV inverter output filter inductance (i.e.,  $L + L_g$ ) is less than 0.1 pu, in order to limit the ac voltage drop during operation; and
- 4) the reactive power of the *LCL*-filter capacitor  $C_f$  is less than 5% of the rated power, in order to limit the power factor decrease at rated power.

During the execution of the proposed optimization process, the components considered each time for incorporation in the PV inverter structure are evaluated according to: 1) their cost [i.e., parameters  $c_s$ ,  $c_i$ , etc., in (4)]; 2) their resulting failure rates incorporated in (7), which in turn affect the total maintenance cost of the PV inverter according to (5); and iii) their power losses which affect the energy production of the PV inverter according to (14) and (15).

#### IV. OPTIMIZATION EXAMPLE

As an optimization example, a 2 kW/220 V transformerless, full-bridge, grid-connected PV inverter, which is illustrated in Fig. 1, has been optimally designed using the proposed methodology. The PV array connected to the PV inverter is comprised of 12 175 W/35.4 V (under standard test conditions) PV modules connected in series. The PV modules' annual output power reduction coefficient, specified by their manufacturer, is equal to  $r(y) = 0.6\%$ . The PV system service lifetime considered in the optimization process is  $n = 25$  years.

As analyzed in Section II, the proposed optimization procedure can be performed considering multiple alternative types of PV inverter components (i.e., power switches, heat sinks, etc.) in order to derive the overall optimum PV inverter configuration. In this design example, the PV inverter power section is built using IGBT-type power switches with free-wheeling diodes. In order to demonstrate the features of the proposed methodology and explore the effect of the heat sink type on the PV inverter reliability characteristics during the execution of the proposed optimal design process, the IGBT-type power switches and free-wheeling diodes have been considered to be mounted on two alternative types of heat sinks with dissimilar cost and thermal conduction characteristics, expressed by  $c_{hs}$  and  $\theta_{ca}$  in (4), and (8) and (9), respectively. The technical and economical characteristics of commercially available components used to build the PV inverter power section and output filter (i.e., heat sinks, IGBTs, inductors, etc.), which are input in the optimization process illustrated in Fig. 2, are summarized in Tables I and II, respectively. The technical characteristics of the PV inverter components were based on the information provided by their

TABLE I  
TECHNICAL CHARACTERISTICS OF THE PV INVERTER COMPONENTS

$\theta_{ca}$ ( $\frac{^{\circ}\text{C}}{\text{W}}$ )	$\theta_{jc,ps}$ ( $\frac{^{\circ}\text{C}}{\text{W}}$ )	$T_{jps,max}$ ( $^{\circ}\text{C}$ )	$\theta_{jc,d}$ ( $\frac{^{\circ}\text{C}}{\text{W}}$ )	$T_{jd,max}$ ( $^{\circ}\text{C}$ )	$f_{s,max}$ (kHz)	$S_i$ ( $\frac{\text{m}^2}{\text{H}\cdot\text{A}}$ )
Type 1: 0.65	1.7	175	2.6	175	30	5.1
Type 2: 0.29						

TABLE II  
ECONOMICAL CHARACTERISTICS OF THE PV INVERTER COMPONENTS

$c_{inv}$ ( $\frac{\text{€}}{\text{W}}$ )	$c_{hs}$ (€)	$c_s + c_d$ (€)	$c_i$ ( $\frac{\text{€}}{\text{H}\cdot\text{A}}$ )	$c_c$ ( $\frac{\text{€}}{\text{F}}$ )	$c_r$ ( $\frac{\text{€}}{\Omega\cdot\text{W}}$ )	$M_{inv}$ (€)	$g$ (%)	$d$ (%)
280.4	Type 1: 27.2	1.5	832	$134\cdot 10^3$	$3.6\cdot 10^{-3}$	100.0	3.0	5.0
	Type 2: 87.5							

manufacturers. The economical characteristics of the PV inverter components considered in the optimization process are based on the selling prices of the corresponding components in the international market, also considering that a large volume of components is expected to be purchased during the industrial construction of the PV inverter.

The maximum permissible limit of harmonic current distortion at the PV inverter output  $RF_{max}$  has been set equal to 4%. The total failure rate of the PV inverter components not included in the set of the PV inverter design variables (e.g., FPGA or DSP boards, monitoring sensors, etc.) has been set equal to  $\lambda_c = 17.2$  failures/ $10^6$  h [28], [34]. It is assumed that the PV inverter repair time is zero, in order to derive results independent of factors which are not directly related to the PV inverter design process, such as the geographic isolation of the PV system installation site, maintenance personnel and spare parts availability [28], etc.

A software program operating under the MATLAB platform has been developed for the implementation of the proposed optimal design method. The global minimum of the PV inverter LCOE (objective) function is calculated using the genetic algorithm functions available in the MATLAB Global Optimization Toolbox.

The proposed methodology has been applied for the design optimization of PV inverters installed at various sites in Europe. The resulting optimal values of the PV inverter design variables (i.e.,  $L$ ,  $L_g$ ,  $C_f$ ,  $R_{dr}$ , and  $f_s$ ) and LCOE for both alternative types of heat sinks input in the proposed design optimization process are presented in Table III. A different set of optimal values has been derived for each type of heat sink deployed in the PV inverter structure since different solar irradiation and ambient temperature conditions prevail at each installation site, which affect both the total PV energy production and the PV inverter reliability performance. Thus, the technical and economical characteristics of the heat sink impact the optimal values of the *LCL*-filter components which are required in order to obtain the minimization of the PV inverter LCOE.

TABLE III  
OPTIMAL VALUES OF THE PV INVERTER DESIGN VARIABLES AND LCOE FOR  
VARIOUS INSTALLATION SITES IN EUROPE

		Heat sink	$L$ (mH)	$L_g$ ( $\mu$ H)	$C_f$ ( $\mu$ F)	$R_{dr}$ ( $\Omega$ )	$f_s$ (kHz)	LCOE ( $\frac{\epsilon}{\text{MWh}}$ )
Athens (Greece)	Type 1		1.481	83.086	4.484	4.189	29.95	15.051
	Type 2		1.726	54.326	4.112	3.579	29.95	16.400
Murcia (Spain)	Type 1		1.413	52.360	5.065	3.157	29.95	13.249
	Type 2		1.481	54.386	4.827	3.297	29.95	14.404
Freiburg (Germany)	Type 1		1.466	49.305	5.125	3.051	29.90	21.910
	Type 2		1.463	45.366	5.519	2.824	29.95	23.776
Oslo (Norway)	Type 1		1.573	49.573	4.887	3.136	29.95	22.277
	Type 2		1.602	49.438	4.801	3.161	29.95	24.200

For the specific operational and economical characteristics of the components considered in the optimization example (see Tables I and II), the manufacturing cost per unit power of the optimized PV inverters presented in Table III using heat sink type-1 is 30.29–30.35 cents of  $\epsilon/\text{W}$ , while the corresponding values in case that heat sink type-2 is used are in the range of 33.32–33.42 cents of  $\epsilon/\text{W}$ . The manufacturing cost of the optimized PV inverter can be further reduced in order to achieve the desirable economic targets by building the inverter using components with lower selling prices.

During the design of a PV inverter, it is not generally known *a priori* by how much the switching frequency should be increased since this also increases the switching losses of the power semiconductors. The proposed methodology enables us to explore the impact of the PV inverter component values on the lifetime-cost/power-losses tradeoff in order to derive the overall optimal PV inverter configuration providing the minimum LCOE. For the specific operational and economical characteristics of the components considered in this optimization example (see Tables I and II), the optimal value of the switching frequency  $f_s$  in Table III has been calculated to be close to the maximum permissible switching frequency of the IGBT-type power switches considered, thus aiming toward the reduction of the *LCL*-filter size and cost.

According to Table I, the thermal resistance of heat sink type 1 is higher compared to that of heat sink type 2, resulting in the development of higher junction temperatures in the power semiconductors. Depending on the installation area, the resulting failure rates of the IGBT power switches and diodes in the optimized PV inverters presented in Table III, which have been built using heat sink type 1, are 146.58–146.71 and 99.33–104.48 failures/ $10^9$  h, respectively. These values are higher by 0.02–0.019% and 0.003–0.01%, respectively, compared to the case that heat sink type 2 is used. The failure rates of the optimized PV inverters for both heat sink types in each installation site are depicted in Fig. 4. It is observed that different values of the total failure rates of the optimized PV inverters resulted in each installation site since: 1) a different set of optimal values

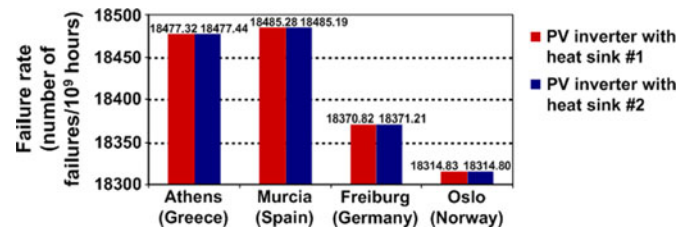


Fig. 4. Failure rates of the optimized PV inverters for both heat sink types in each installation site.

of the PV inverter components (i.e., design variables) has been derived for each type of heat sink employed in the PV inverter structure in order to minimize the LCOE of the corresponding PV inverter, as presented in Table III; and 2) different meteorological conditions prevail in each installation area, which affect the stress factors applied at the individual components of the PV inverter. As analyzed in Section III, the failure rates are calculated using the average values of the stress factors applied at each component, weighted by the percentage of operating hours at each stress level. This process smoothes the impact of extreme individual values of the stress factors on the resulting failure rate. Thus, in each installation site the total failure rates and lifetime maintenance costs which resulted for the PV inverters using either of the two heat sink types considered do not differ significantly. However, the heat sink of type 1 is of much lower cost compared to the type 2 heat sink, thus constituting the optimal heat sink type which provides the minimum LCOE in all installation sites, as illustrated in Table III. The failure rate is a statistical parameter and the number of failures experienced by the PV inverter under actual operating conditions depends on the probability that the PV inverter will operate properly beyond time  $t$ , as expressed by (6). Thus, in the proposed optimization methodology, the average number of failures during each year of operation is calculated by performing a Monte Carlo simulation, as described in Section III.

The optimal values of LCOE and the total energy injected into the electric grid during the 25-year operational lifetime period [i.e.,  $E_i$  in (2) and (14)] of a PV inverter built using heat sink of type-1, which is the optimal type of heat sink as analyzed previously, for various installation sites in Europe, are depicted in Fig. 5(a) and (b), respectively. It is observed that the overall minimum LCOE and the maximum energy production are achieved in Murcia, Spain, since that installation site exhibits the highest solar irradiation potential.

The optimal values of the MTBF [27] of the PV inverters optimized for each installation site are presented in Fig. 5(c). It is observed that although the PV inverter optimized for Murcia, Spain, achieves the overall minimum LCOE, it also exhibits the minimum optimal MTBF among the PV inverters optimized for each installation site. This is due to the higher solar irradiation and ambient temperature operating conditions prevailing at this installation site, resulting in increased values of the stress factors, which adversely affect the PV inverter reliability performance. The maximum deviation of the calculated optimal MTBF values among the four installation sites is 0.9%.

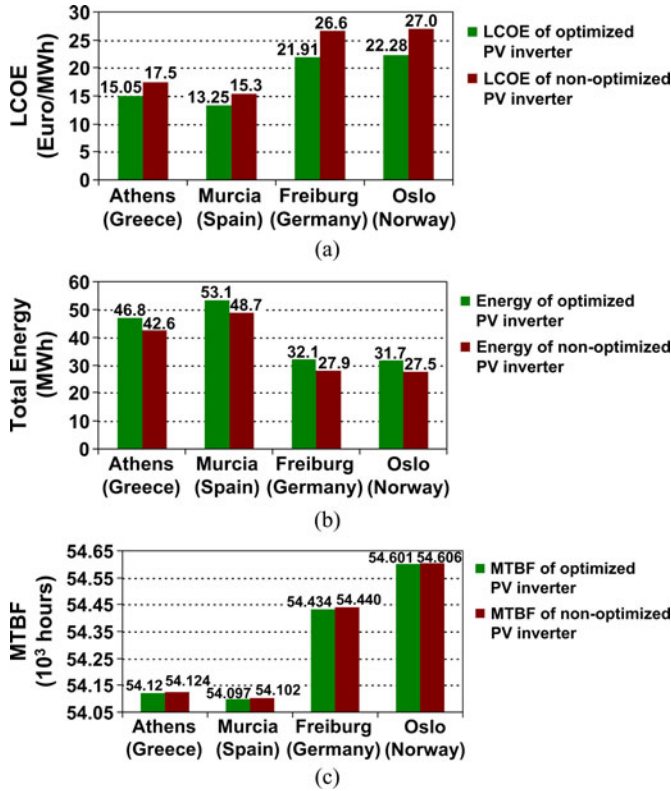


Fig. 5. Performance of the optimized and nonoptimized PV inverters for various installation sites in Europe: (a) LCOE, (b) total energy injected into the electric grid for 12 PV modules during the 25-year operational lifetime period, and (c) mean time between failures.

The case that the single-phase, full-bridge PV inverter under study is designed without using the proposed optimization process, thus forming a nonoptimized PV inverter, has also been considered for comparison purposes. The manufacturing cost, lifetime energy production, and reliability features have not been considered during the design process of the nonoptimized PV inverter. The nonoptimized PV inverter operates at  $f_s = 8$  kHz, which is the typical switching frequency value in this power range [2], [41]. Also, it is comprised of type-1 heat sink and an  $LCL$  output filter, which has been designed as analyzed in [5], with  $L = 5.65$  mH,  $L_g = 1.09$  mH,  $C_f = 3.29$   $\mu$ F, and  $R_{dr} = 5.6$   $\Omega$ . The rest of the nonoptimized PV inverter specifications (i.e., power rating, output frequency, etc.) are identical to those of the PV inverter which has been optimally designed using the proposed methodology. Comparing the individual values of the design variables in the nonoptimized PV inverter and the corresponding optimal values derived using the proposed methodology for a PV inverter comprised of type-1 heat sink, which are presented in Table III, a significant deviation is observed. The average deviations for all installation sites of the corresponding values of the  $L$ ,  $L_g$ ,  $C_f$ ,  $R_{dr}$ , and  $f_s$  design variables in the optimized and nonoptimized PV inverters are 73.75%, 94.63%, 48.64%, 39.58%, and 274.22%, respectively, thus demonstrating the strength of the proposed design methodology to facilitate the optimal design of the PV inverter based on a systematic process. The LCOE, total energy pro-

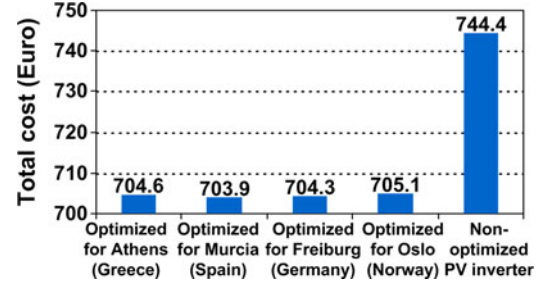


Fig. 6. Total cost of the optimized and nonoptimized PV inverters for various installation sites in Europe.

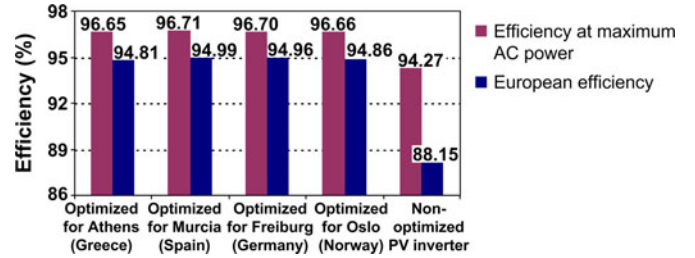


Fig. 7. Efficiency at maximum ac power and European efficiency of PV inverters optimized for various installation sites in Europe and of the nonoptimized PV inverter.

duction, and MTBF of the nonoptimized PV inverter are also presented in Fig. 5. As shown in Fig. 5(c), compared to the optimized PV inverters designed using the proposed methodology, the nonoptimized PV inverter exhibits slightly higher MTBF in all installation sites considered. However, such a deviation does not significantly affect the resulting lifetime maintenance cost of the nonoptimized PV inverter. Thus, compared to the nonoptimized PV inverter, the LCOE of the optimized PV inverters is lower by 13.4–17.6% [see Fig. 5(a)] and the total energy injected into the electric grid is higher by 9–15% [see Fig. 5(b)].

The present value of the PV inverter total cost [i.e.,  $C_{inv}$  in (2) and (3)] of the optimized and nonoptimized PV inverters is illustrated in Fig. 6. In all cases considered, the maintenance cost corresponds to approximately 13.9% of the PV inverter total cost. Thus, the variation of the optimal total cost among the four installation sites is practically due to the different values of the components required to build the optimized PV inverter in each site (see Table III), which affect the corresponding manufacturing costs. Compared to the nonoptimized PV inverter, the total cost of the optimized PV inverters is lower by 5.6–5.7%. The manufacturing cost per unit power of the nonoptimized PV inverter is 32.31 cents of €/W and it is higher than the corresponding cost of the optimized PV inverter using heat sink type 1 by 6.47–6.67%.

The efficiency at maximum ac power and European efficiency of the optimized and nonoptimized PV inverters, for various installation sites in Europe, are presented in Fig. 7. Compared to the nonoptimized PV inverter, the efficiency at maximum ac power and European efficiency of the PV inverters designed using the proposed methodology are higher by 2.52–2.59% and 7.55–7.75%, respectively. The PV inverter optimized for Murcia, Spain, achieves the highest values of efficiency at

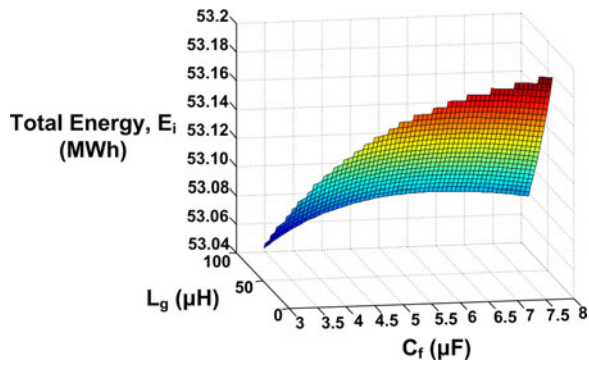


Fig. 8. Variation of the total energy injected into the electric grid by a PV inverter installed in Murcia, Spain, for various values of the design variables  $L_g$  and  $C_f$ , in the case that  $L = 1.413$  mH and  $f_s = 29.95$  kHz.

maximum ac power and European efficiency and simultaneously, as demonstrated in Fig. 6, exhibits the lowest lifetime cost.

The variation of the total energy injected into the electric grid [i.e.,  $E_i$  in (2) and (14)] by a PV inverter installed in Murcia, Spain, for various values of the design variables  $L_g$  and  $C_f$  in the case that  $L = 1.413$  mH and  $f_s = 29.95$  kHz, is illustrated in Fig. 8. It is observed that  $E_i$  is a highly nonlinear function of the values of the PV inverter components, thus dictating the use of a computationally efficient optimization algorithm, such as GAs, in order to calculate the optimal value of the PV inverter LCOE. The successful detection by the GA-based optimization procedure of the global optimum point where the PV inverter LCOE is minimized has been verified by also performing the proposed optimization process using an exhaustive search procedure.

## V. CONCLUSION

Targeting at cost-effective deployment of grid-connected PV systems, a new methodology for the optimal design of transformerless PV inverters has been presented in this paper. The optimal switching frequency as well as the optimal values and types of the components comprising the PV inverter is calculated such that the PV inverter LCOE generated is minimized. The LCOE is calculated also considering the PV inverter component reliability in terms of the corresponding failure rates, which affect the lifetime maintenance cost of the PV inverter.

The proposed design method facilitates the optimal design of the PV inverter based on a systematic process. The design optimization results indicate that in contrast to the past-proposed design approaches, the methodology presented in this paper has the advantage of enabling to explore the impact of the PV inverter component values on the lifetime-cost/power-losses tradeoff in order to derive the overall optimal PV inverter configuration, while simultaneously considering the PV inverter components reliability which affects the lifetime maintenance cost of the PV inverter. The optimal values of the PV inverter design parameters depend also on the meteorological conditions prevailing at the PV system installation site. Compared to the nonoptimized PV inverter structures, the PV inverters designed using

the proposed methodology exhibit lower total cost (including the manufacturing and lifetime maintenance costs) and inject more energy into the electric grid.

## REFERENCES

- [1] European Photovoltaic Industry Association. (2011, May). Global market outlook for photovoltaics until 2015 [Online]. Available: <http://www.epia.org>
- [2] T. Kerekes, R. Teodorescu, P. Rodríguez, G. Vázquez, and E. Aldabas, "A new high-efficiency single-phase transformerless PV inverter topology," *IEEE Trans. Ind. Electron.*, vol. 58, no. 1, pp. 184–191, Jan. 2011.
- [3] H. Xiao and S. Xie, "Transformerless split-inductor neutral point clamped three-level PV grid-connected inverter," *IEEE Trans. Power Electron.*, vol. 27, no. 4, pp. 1799–1808, Apr. 2012.
- [4] H. Cha and T.-K. Vu, "Comparative analysis of low-pass output filter for single-phase grid-connected Photovoltaic inverter," in *Proc. 25th Annu. IEEE Appl. Power Electron. Conf. Expos.*, 2010, pp. 1659–1665.
- [5] M. Liserre, F. Blaabjerg, and S. Hansen, "Design and control of an LCL-filter-based three-phase active rectifier," *IEEE Trans. Ind. Appl.*, vol. 41, no. 5, pp. 1281–1291, Sep. 2005.
- [6] O. Haillant, "Accelerated weathering testing principles to estimate the service life of organic PV modules," *Solar Energy Mater. Solar Cells*, vol. 95, no. 5, pp. 1284–1292, May 2011.
- [7] J. M. Fife, M. Scharf, S. G. Hummel, and R. W. Morris, "Field reliability analysis methods for photovoltaic inverters," in *Proc. 35th IEEE Photovoltaic Spec. Conf. (PVSC)*, Jun. 2010, pp. 2767–2772.
- [8] R. Kadri, J.-P. Gaubert, and G. Champenois, "An improved maximum power point tracking for photovoltaic grid-connected inverter based on voltage-oriented control," *IEEE Trans. Ind. Electron.*, vol. 58, no. 1, pp. 66–75, Jan. 2011.
- [9] E. Koutroulis and F. Blaabjerg, "Design optimization of grid-connected PV inverters," in *Proc. 26th Annu. IEEE Appl. Power Electron. Conf. Expos.*, Mar. 2011, pp. 691–698.
- [10] P. Chaparala, E. Li, and S. Bhola, "Reliability qualification of photovoltaic smart panel electronics," in *Proc. 17th IEEE Int. Symp. Phys. Failure Anal. Integr. Circuits*, Jul. 2010, pp. 1–4.
- [11] G. Petrone, G. Spagnuolo, R. Teodorescu, M. Veerachary, and M. Vitelli, "Reliability issues in photovoltaic power processing systems," *IEEE Trans. Ind. Electron.*, vol. 55, no. 7, pp. 2569–2580, Jul. 2008.
- [12] J. M. Fife and R. W. Morris, "System availability analysis for a multi-megawatt photovoltaic power plant," in *Proc. 34th IEEE Photovolt. Spec. Conf.*, Jun. 2009, pp. 1221–1226.
- [13] S. V. Dhople and A. D. Dominguez-Garcia, "Estimation of photovoltaic system reliability and performance metrics," *IEEE Trans. Power Syst.*, vol. 27, no. 1, pp. 554–563, Feb. 2012.
- [14] Z. J. Ma and S. Thomas, "Reliability and maintainability in photovoltaic inverter design," in *Proc. Annu. Reliab. Maintainability Symp.*, 2011, pp. 1–5.
- [15] Y. Xue, K. C. Divya, G. Griepentrog, M. Liviu, S. Suresh, and M. Manjrekar, "Towards next generation photovoltaic inverters," in *Proc. IEEE Energy Convers. Congr. Expo.*, Sep. 2011, pp. 2467–2474.
- [16] G. Petrone and G. Spagnuolo, "Recent advances in efficient and reliable photovoltaic systems," in *Proc. 37th Annu. Conf. IEEE Ind. Electron. Soc.*, Nov. 2011, pp. 4619–4622.
- [17] H. Preckwinkel, D. V. M. M. Krishna, N. Frohliche, and J. Bocker, "Photovoltaic inverter with high efficiency over a wide operation area—A practical approach," in *Proc. 37th Annu. Conf. IEEE Ind. Electron. Soc.*, Nov. 2011, pp. 912–917.
- [18] A. Nanakos, E. Tatakis, and N. Papanikolaou, "A weighted-efficiency oriented design methodology of flyback inverter for AC photovoltaic modules," *IEEE Trans. Power Electron.*, vol. 27, no. 7, pp. 3221–3233, Jul. 2012.
- [19] S. Yang, D. Xiang, A. Bryant, P. Mawby, L. Ran, and P. Tavner, "Condition monitoring for device reliability in power electronic converters: A review," *IEEE Trans. Power Electron.*, vol. 25, no. 11, pp. 2734–2752, Nov. 2010.
- [20] D. Hirschmann, D. Tissen, S. Schroder, and R. W. De Doncker, "Reliability prediction for inverters in hybrid electrical vehicles," *IEEE Trans. Power Electron.*, vol. 22, no. 6, pp. 2511–2517, Nov. 2007.
- [21] X. Yu and A. Khambadkone, "Reliability analysis and cost optimization of parallel inverter system," *IEEE Trans. Ind. Electron.*, vol. 59, no. 10, pp. 3881–3889, Oct. 2012.
- [22] S. V. Dhople, A. Davoudi, A. D. Domínguez-García, and P. L. Chapman, "A unified approach to reliability assessment of multiphase DC–DC

- converters in photovoltaic energy conversion systems," *IEEE Trans. Power Electron.*, vol. 27, no. 2, pp. 739–751, Feb. 2012.
- [23] F. Chan and H. Calleja, "Design strategy to optimize the reliability of grid-connected PV systems," *IEEE Trans. Ind. Electron.*, vol. 56, no. 11, pp. 4465–4472, Nov. 2009.
- [24] S. Harb and R. S. Balog, "Reliability of candidate photovoltaic module-integrated-inverter topologies," in *Proc. 27th Annu. IEEE Appl. Power Electron. Conf. Expo.*, Feb. 2012, pp. 898–903.
- [25] S. J. Castillo, R. S. Balog, and P. Enjeti, "Predicting capacitor reliability in a module-integrated photovoltaic inverter using stress factors from an environmental usage model," in *Proc. North Amer. Power Symp.*, 2010, pp. 1–6.
- [26] C. J. Murray, A. Davoudi, and P. L. Chapman, "Reliability analysis for single-phase photovoltaic inverters with reactive power support," in *Proc. IEEE Power Energy Conf. Illinois*, Feb. 2011, pp. 1–6.
- [27] F. Chan and H. Calleja, "Reliability estimation of three single-phase topologies in grid-connected PV systems," *IEEE Trans. Ind. Electron.*, vol. 58, no. 7, pp. 2683–2689, 2011.
- [28] A. Ristow, M. Begovic, A. Pregelj, and A. Rohatgi, "Development of a methodology for improving photovoltaic inverter reliability," *IEEE Trans. Ind. Electron.*, vol. 55, no. 7, pp. 2581–2592, Jul. 2008.
- [29] L. Battistelli, E. Chiodo, and D. Lauria, "Bayes assessment of photovoltaic inverter system reliability and availability," in *Proc. Int. Symp. Power Electron. Electric. Drives Autom. Motion (SPEEDAM)*, 2010, pp. 628–634.
- [30] S. V. Dhople, A. Davoudi, P. L. Chapman, and A. D. Domínguez-García, "Integrating photovoltaic inverter reliability into energy yield estimation with Markov models," in *Proc. IEEE 12th Workshop Control Model. Power Electron.*, Jun. 2010, pp. 1–5.
- [31] M. Campbell, J. Blunden, E. Smeloff, and P. Aschenbrenner, "Minimizing utility-scale PV power plant LCOE through the use of high capacity factor configurations," in *Proc. 34th IEEE Photovoltaic Spec. Conf.*, Jun. 2009, pp. 421–426.
- [32] Department of Defense, *Reliability Prediction of Electronic Equipment*, Military Handbook 217-F, USA 1991.
- [33] A. M. Bazzi, A. Dominguez-Garcia, and P. T. Krein, "Markov reliability modeling for induction motor drives under field-oriented control," *IEEE Trans. Power Electron.*, vol. 27, no. 2, pp. 534–546, Feb. 2012.
- [34] M. Aten, G. Towers, C. Whitley, P. Wheeler, J. Clare, and K. Bradley, "Reliability comparison of matrix and other converter topologies," *IEEE Trans. Aerosp. Electron. Syst.*, vol. 42, no. 3, pp. 867–875, Jul. 2006.
- [35] C. Rodriguez and G. A. J. Amaratunga, "Energy control for long lifetime photovoltaic ac module inverter," in *Proc. 37th IEEE Power Electron. Spec. Conf.*, Jun. 2006, pp. 1–6.
- [36] E. Koutroulis and F. Blaabjerg, "Techniques for the optimal design of photovoltaic inverters interconnected with the electric grid," in *Proc. 14th Eur. Conf. Power Electron. Appl.*, 2011, pp. 1–10.
- [37] S. K. Pattnaik and K. K. Mahapatra, "Power loss estimation for PWM and soft-switching inverter using RDCLI," in *Proc. Int. MultiConf. Eng. Comput. Sci.*, 2010, pp. 1401–1406.
- [38] C. R. Osterwald and T. J. McMahon, "History of accelerated and qualification testing of terrestrial photovoltaic modules: A literature review," *Prog. Photovolt.: Res. Appl.*, vol. 17, no. 1, pp. 11–33, Jan. 2009.
- [39] E. Lorenzo, *Solar Electricity: Engineering of Photovoltaic Systems*, 1st ed. Sevilla, Spain: Progensa, 1994, pp. 87–99.
- [40] N. Mohan, T. M. Undeland, and W. P. Robbins, *Power Electronics: Converters, Applications, and Design*, 2nd ed. Hoboken, NJ: Wiley, 1995, pp. 211–218.
- [41] H. F. Xiao, S. J. Xie, C. Yang, and R. H. Huang, "An optimized transformerless photovoltaic grid-connected inverter," *IEEE Trans. Ind. Electron.*, vol. 58, no. 5, pp. 1887–1895, May 2011.



**Eftichios Koutroulis** (M'10) was born in Chania, Greece, in 1973. He received the B.Sc. and M.Sc. degrees from the Department of Electronic and Computer Engineering, Technical University of Crete, Chania, in 1996 and 1999, respectively. He also received the Ph.D. degree from the Department of Electronic and Computer Engineering, Technical University of Crete, in 2002 in the area of power electronics and renewable energy sources (RES).

He is currently an Assistant Professor at the Department of Electronic and Computer Engineering, Technical University of Crete. His research interests include power electronics (dc/ac inverters, dc/dc converters), the development of microelectronic energy management systems for RES, and the design of photovoltaic and wind energy conversion systems.



**Frede Blaabjerg** (S'86–M'88–SM'97–F'03) received the Ph.D. degree from Aalborg University, Aalborg, Denmark, in 1992.

From 1987 to 1988, he was with ABB-Scandia, Randers. He became an Assistant Professor in 1992, an Associate Professor in 1996, and a Full Professor in power electronics and drives in 1998 at Aalborg University. He has been a Part-Time Research Leader at Research Center Risoe in wind turbines. During 2006–2010, he was the Dean of the Faculty of Engineering, Science and Medicine and became a

Visiting Professor at Zhejiang University, China, in 2009. His research areas include power electronics and its applications such as wind turbines, PV systems, and adjustable speed drives.

Dr. Blaabjerg has been the Editor-in-Chief of the IEEE TRANSACTIONS ON POWER ELECTRONICS since 2006. He was a Distinguished Lecturer for the IEEE Power Electronics Society during 2005–2007 and for the IEEE Industry Applications Society during 2010–2011. He received the 1995 Angelos Award for his contribution in modulation technique and the Annual Teacher prize at Aalborg University. He also received the Outstanding Young Power Electronics Engineer Award from the IEEE Power Electronics Society in 1998. He has received ten IEEE Prize paper awards and another prize paper award at PELINCEC Poland 2005. He received the IEEE PELS Distinguished Service Award in 2009 and the EPE-PEMC 2010 Council award.